

Supplementary Materials for  
Ocean weather systems on icy moons, with application to Enceladus

Yixiao Zhang *et al.*

Corresponding author: Yixiao Zhang, [yixiaoz@mit.edu](mailto:yixiaoz@mit.edu)

*Sci. Adv.* **10**, eadn6857 (2024)  
DOI: 10.1126/sciadv.adn6857

**This PDF file includes:**

Supplementary Text  
Figs. S1 to S4

## Supplementary Text

### Diagnosis of overturning Circulation

We diagnose the streamfunction,  $\Psi^*$ , from the eddy heat transport (29,47):

$$\Psi^* = -\frac{\overline{w'T'}}{\partial_y \overline{T}}, \quad (\text{S1})$$

where  $\overline{w'T'}$  is the vertical component of eddy heat flux. This residual circulation transport heat both equatorward and upward, in a direction that is almost aligned with  $\overline{T}$  surfaces (Fig. 5(A)).

$$(\overline{w'T'})_{\text{skew}} = -\Psi^* \partial_y \overline{T} \quad (\text{S2})$$

$$(\overline{v'T'})_{\text{skew}} = \Psi^* \partial_z \overline{T} \quad (\text{S3})$$

To see how much of the total heat transport is captured by the skew flux induced by  $\Psi^*$ , we compute the difference between the two, i.e., the residual fluxes:

$$(\overline{w'T'})_{\text{residual}} = \overline{w'T'} - (\overline{w'T'})_{\text{skew}} \quad (\text{S4})$$

$$(\overline{v'T'})_{\text{residual}} = \overline{v'T'} - (\overline{v'T'})_{\text{skew}} \quad (\text{S5})$$

### Temperature coordinates

To transform Eq. (14), which uses the Cartesian coordinates ( $y$  and  $z$ ), to temperature coordinates ( $y$  and  $T$ ), we start from the horizontal and vertical gradients of a scale  $\phi$  given the chain rule:

$$(\partial_y \phi)_z = (\partial_y \phi)_T - \frac{(\partial_y z)_T}{\partial_T z} \partial_T \phi \quad (\text{S6})$$

$$\partial_z \phi = \frac{\partial_T \phi}{\partial_T z} \quad (\text{S7})$$

where the subscripts represent the vertical coordinates used.

The left-hand side of Eq. (14) becomes

$$\begin{aligned}
J(\Psi^*, T) &= (\partial_y \Phi^*)_z \partial_z T - \partial_z \Psi^* (\partial_y T)_z \\
&= \left( (\partial_y \Psi^*)_T - \frac{(\partial_y z)_T}{\partial_T z} \partial_T \Psi^* \right) \frac{\partial_T T}{\partial_T z} - \left( (\partial_y T)_T - \frac{(\partial_y z)_T}{\partial_T z} \partial_T T \right) \frac{\partial_T \Psi^*}{\partial_T z} \\
&= \left( (\partial_y \Psi^*)_T - \frac{(\partial_y z)_T}{\partial_T z} \partial_T \Psi^* \right) \frac{1}{\partial_T z} - \left( -\frac{(\partial_y z)_T}{\partial_T z} \partial_T T \right) \frac{\partial_T \Psi^*}{\partial_T z} \\
&= \frac{1}{\partial_T z} (\partial_y \Psi^*)_T
\end{aligned} \tag{S8}$$

Note  $\partial_T T = 1$  and  $(\partial_y T)_T = 0$ .

The slope of the mean temperature surfaces,  $s$ , can be expressed intuitively:

$$s = (\partial_y z)_T \tag{S9}$$

which can be verified with the chain rule (Eq. (S6) and Eq. (S7)).

With the formula for  $\Psi^*$  (Eq. (15)),  $J(\Psi^*, T)$  becomes

$$J(\Psi^*, T) = \frac{K}{\partial_T z} (\partial_y^2 z)_T \tag{S10}$$

The right-hand side of Eq. (14) becomes

$$\begin{aligned}
\kappa \partial_z^2 T &= \frac{\kappa}{\partial_T z} \partial_T \left( \frac{\partial_T T}{\partial_T z} \right) \\
&= \frac{\kappa}{\partial_T z} \partial_T \left( \frac{1}{\partial_T z} \right) \\
&= -\kappa \frac{\partial_T^2 z}{(\partial_T z)^3}
\end{aligned} \tag{S11}$$

Substituting Eq. (S10) and Eq. (S11) into Eq. (14), we arrive at Eq. (16).

## Role of Ekman Pumping

Although the Eulerian-mean overturning circulation is several orders of magnitude weaker than the eddy-driven component, it becomes more important with increased boundary roughness or

decreased vertical diffusivity. Alternating zonal jets can reach several centimeters per second, and top and bottom friction can result in Ekman pumping. We set up two sensitivity tests using a linear boundary drag stress of  $\tau = -\gamma\rho_0u_h$ , where  $\gamma = 10^{-4} \text{ m s}^{-1}$ , which corresponds to a drag coefficient  $c_d \sim 10^{-3}$  and a flow magnitude of  $\sim 1 \text{ cm /s}$ . The first uses  $\Delta T = 0.1 \text{ K}$  and  $\kappa = 10^{-3} \text{ m}^2 \text{ s}^{-1}$ , same as in the control simulation. The zonal jets become weaker, as expected from the additional boundary drag stress. When the non-traditional Coriolis terms can be ignored (as in Earth's ocean, for example), the streamfunction due to Ekman pumping is  $\tau/(\rho_0f)$ . We use the same formula to estimate overturning strength caused by Ekman pumping, and it is broadly in accord with our numerical experiments. We find it is comparable to the eddy-driven overturning circulation. In the second simulation, we use  $\Delta T = 0.1 \text{ K}$  and  $\kappa = 10^{-1} \text{ m}^2 \text{ s}^{-1}$ . In this case, Ekman pumping is weaker than the eddy-driven overturning by  $\sim 2$  orders of magnitude. Because there are complex feedbacks between boundary drag stress, zonal jet velocity, and temperature distribution, we only focus on the case of very weak boundary drag stress in this study.

Temperature ( $^{\circ}$ , Contours) and U ( $\text{m s}^{-1}$ , Shading)

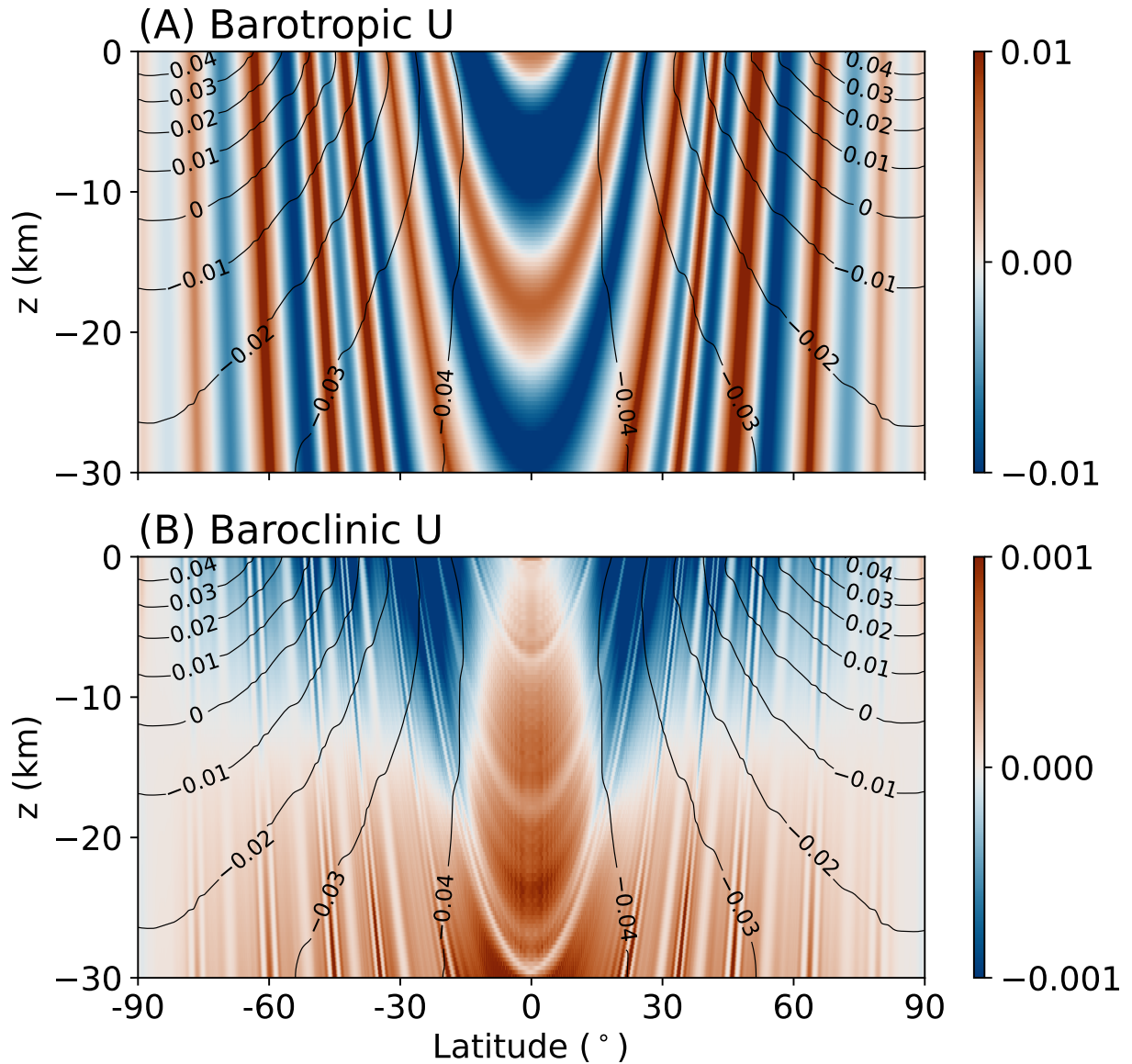


Figure S1: **The barotropic and baroclinic components of the zonal velocity pattern.** Panel (A) shows the barotropic component of  $U$ , which do not vary in the direction of  $f$  and thus do not contribute to thermal wind. Panel (B) shows the baroclinic component. The contours represent isotherms. The barotropic component is stronger than the baroclinic component by approximately one order.

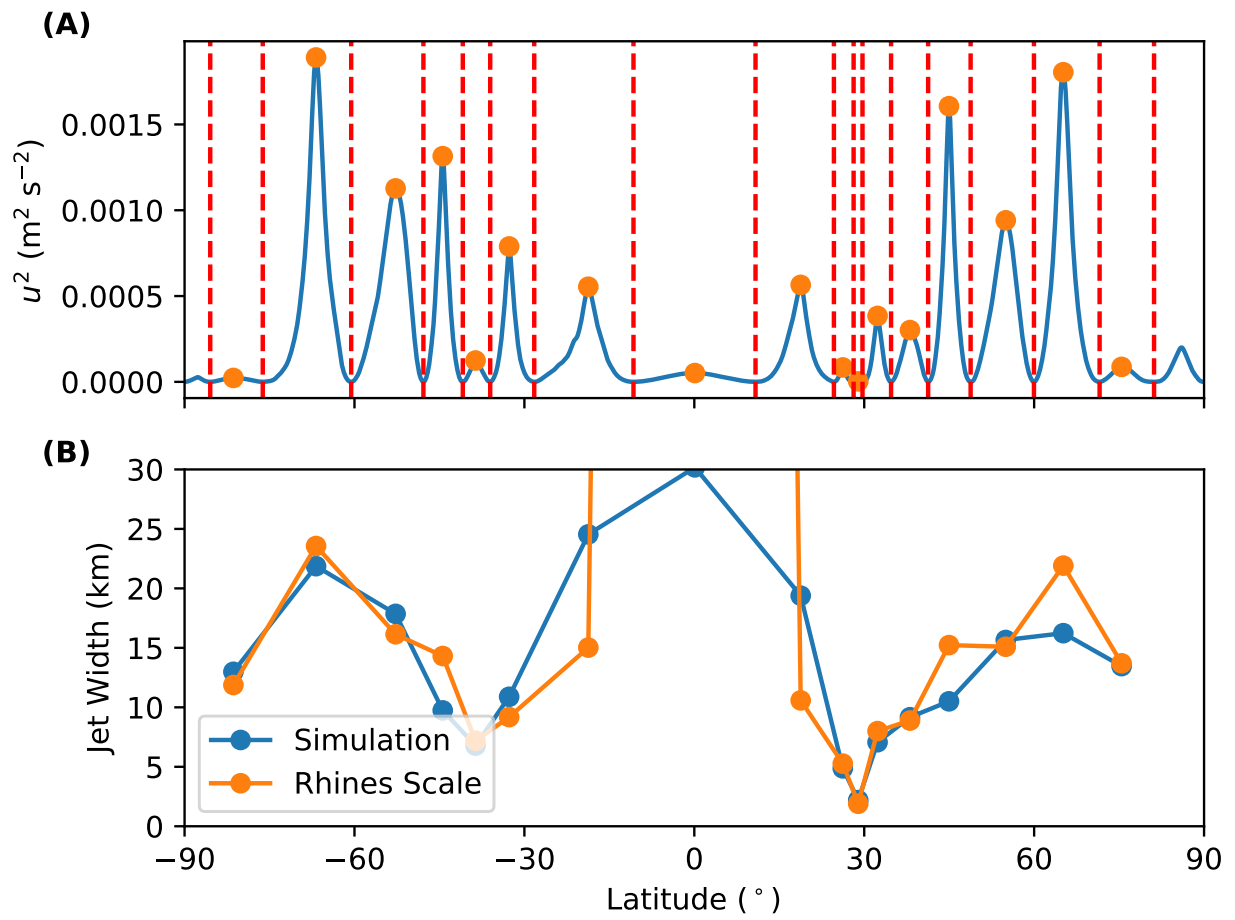


Figure S2: The relationship between the jet widths and the Rhines scale.

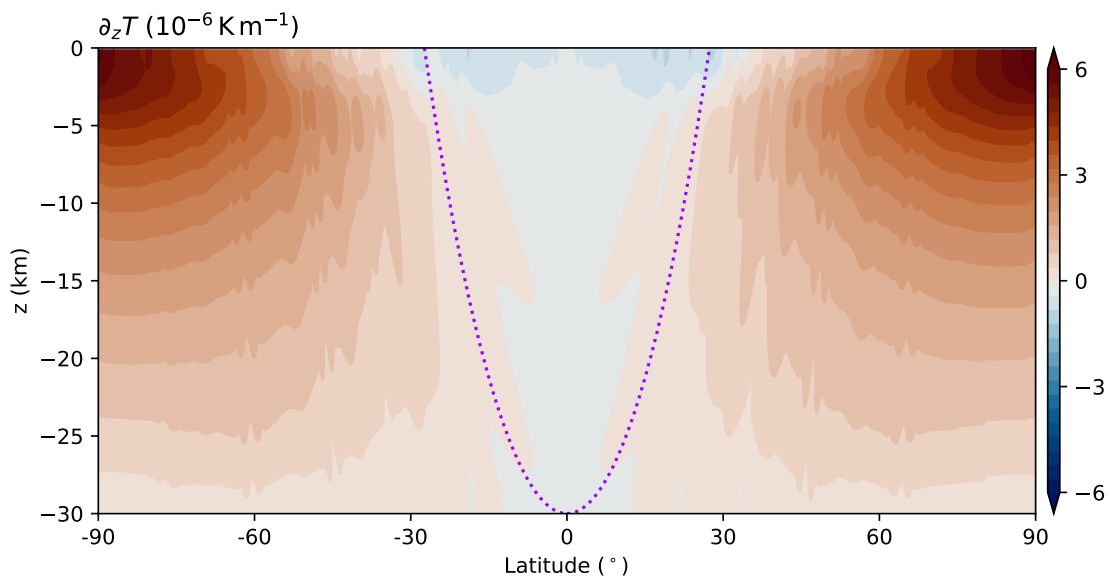


Figure S3: **Vertical temperature in the control simulation.** Reds represent stable stratification and blues represent unstable stratification. The purple dashed line marks the tangent cylinder.

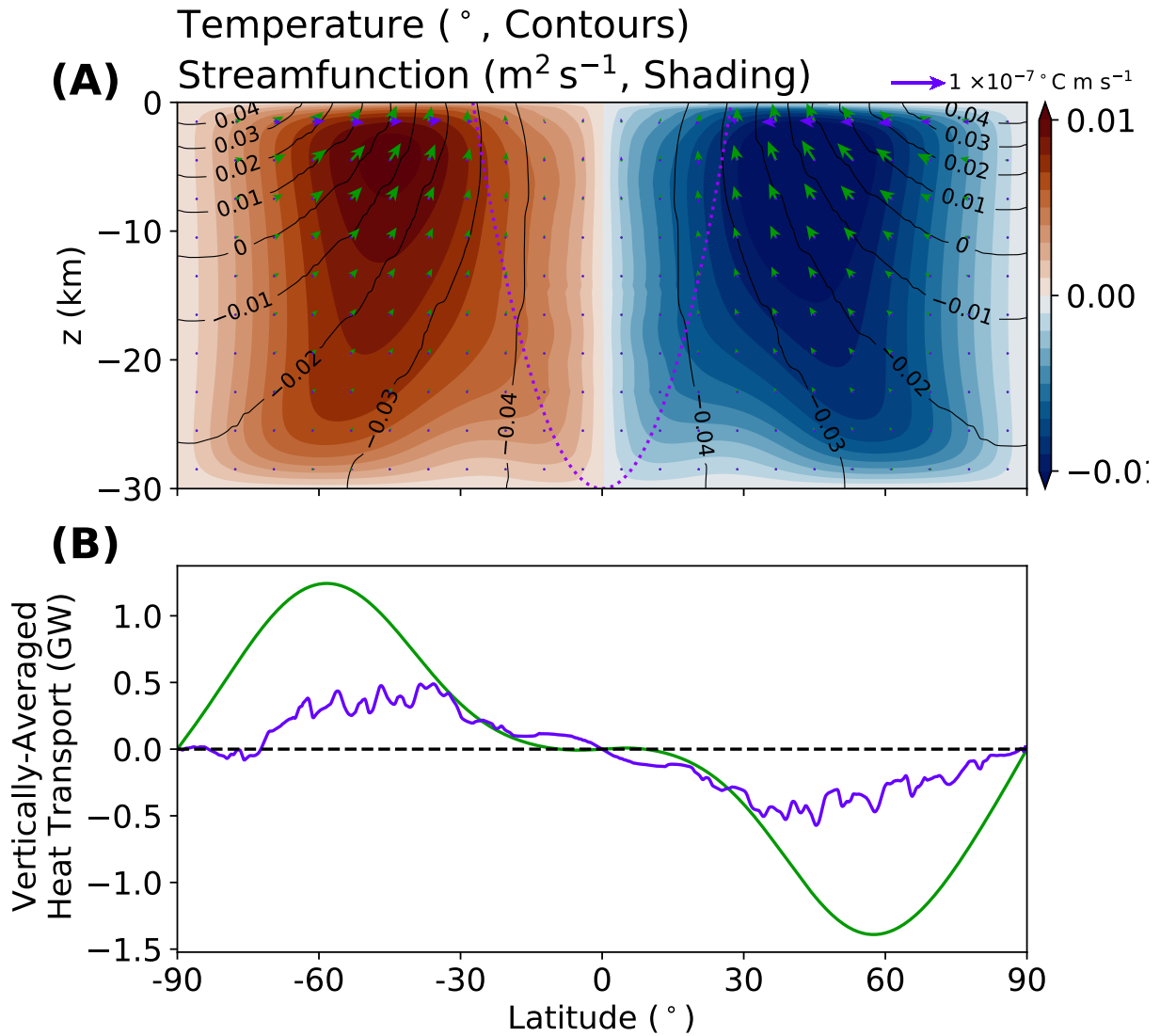


Figure S4: **Skew flux versus residual flux in the control simulation.** Panel (A) is the same as Fig. 5 in the main text. The green arrows in Panel (A) and the green line in Panel (B) represent the skew flux (Eq. (S3),(S2)), while the purple ones represent the residual flux (Eq. (S4),(S5)).